J/ψ production and absorption in pA and d+Au collisions

R. Vogt (LLNL and UC Davis)

In Collaboration with:

C. Lourenço (CERN)

H. Wöhri (LIP and CERN)

R. Nelson (UC Davis and LLNL)

Quarkonium Production Issues

Still Unsettled: Numerous Production Models

Color Evaporation Model (CEM):

Hadronization scale $k = \mathcal{O}(\Lambda_{\rm QCD})$, $Q\overline{Q}$ quantum numbers changed by soft interactions with probabilities specific to each state but independent of energy (Barger *et al.*; Gavai *et al.*; Schuler and RV)

Color Singlet Model I (CSM):

$k = \mathcal{O}(m_Q)$, singlet states with correct quantum numbers; hard gluon needed for S states, *e.g.* $gg \to J/\psi g$; $gg \to \chi_{c2}$ dominant? (Baier *et al.*; Schuler)

Color Singlet Model II (CSM*):

$k = \mathcal{O}(\sqrt{\hat{s}})$, Lansberg *et al.* "$s$-channel cut" diagrams for S states shown to be negligible (Braaten *et al.*)
NLO (+ NNLO*) color singlet contributions seem to fill in gap between LO model and data (Quarkonium Working Group review, in progress)

Nonrelativistic QCD (NRQCD) – alias Color Octet Model:

$k = \mathcal{O}(\alpha_s m_Q)$, $Q\overline{Q}$ quantum numbers changed via gluon emission at bound state momentum scale; corresponds to velocity $v = k/m_Q$ expansion; nonperturbative octet and singlet matrix elements fit to data (Braaten, Bodwin and Lepage; Cho and Leibovich; Beneke and Rothstein; Maltoni *et al.* $\cdots$)

Intrinsic Charm:

k typically assumed to be soft, $gc \to J/\psi c$ provides additional source of high p_T, forward J/ψ production (Brodsky and Lansberg)

Color Evaporation Model

All quarkonium states are treated like $Q\overline{Q}$ ($Q = c, b$) below $H\overline{H}$ ($H = D, B$) threshold

Distributions for all quarkonium family members identical. Production ratios should also be independent of $\sqrt{s}$, p_T, x_F.

At LO, $gg \to Q\overline{Q}$ and $q\overline{q} \to Q\overline{Q}$; NLO add $gq \to Q\overline{Q}q$

$$\sigma_Q^{\rm CEM} = F_Q \sum_{i,j} \int_{4m_Q^2}^{4m_H^2} d\hat{s} \int dx_1 dx_2 \; f_{i/p}(x_1, \mu^2) \; f_{j/p}(x_2, \mu^2) \; \hat{\sigma}_{ij}(\hat{s}) \; \delta(\hat{s} - x_1 x_2 s)$$

Values of m_Q and Q^2 fixed from NLO calculation of $Q\overline{Q}$ production

Main uncertainties arise from choice of PDFs, heavy quark mass, renormalization (α_s) and factorization (evolution of PDFs) scales

Inclusive F_Q fixed by comparison of NLO calculation of $\sigma_Q^{\rm CEM}$ to $\sqrt{s}$ dependence of J/ψ and Υ cross sections, $\sigma(x_F > 0)$ and $Bd\sigma/dy|_{y=0}$ for J/ψ, $Bd\sigma/dy|_{y=0}$ for Υ

Data and branching ratios used to separate the F_Q's for each quarkonium state

Resonance	J/ψ	ψ'	χ_{c1}	χ_{c2}	Υ	Υ'	Υ''	$\chi_b(1P)$	$\chi_b(2P)$
$\sigma_i^{\rm dir}/\sigma_H$	**0.62**	**0.14**	**0.6**	**0.99**	**0.52**	**0.33**	**0.20**	**1.08**	**0.84**
f_i	**0.62**	**0.08**	**0.16**	**0.14**	**0.52**	**0.10**	**0.02**	**0.26**	**0.10**

Table 1: **The ratios of the direct quarkonium production cross sections, $\sigma_i^{\rm dir}$, to the inclusive J/ψ and Υ cross sections, denoted σ_H, and the feed down contributions of all states to the J/ψ and Υ cross sections, f_i, Digal *et al.*.**

Why Still CEM?

Open and hidden charm photo- and hadroproduction show similar energy dependence

High p_T Tevatron Run I data show that, within uncertainties of the data, the prompt J/ψ, the ψ' and χ_c p_T dependencies are the same

Amundsen *et al.* calculated p_T distribution (only partial real part) harder than data at high p_T, undershoots at low p_T – likely because they do not include any k_T smearing

Gavai *et al.* calculated complete J/ψ p_T distribution starting from exclusive NLO $Q\overline{Q}$ production code by Mangano *et al.*

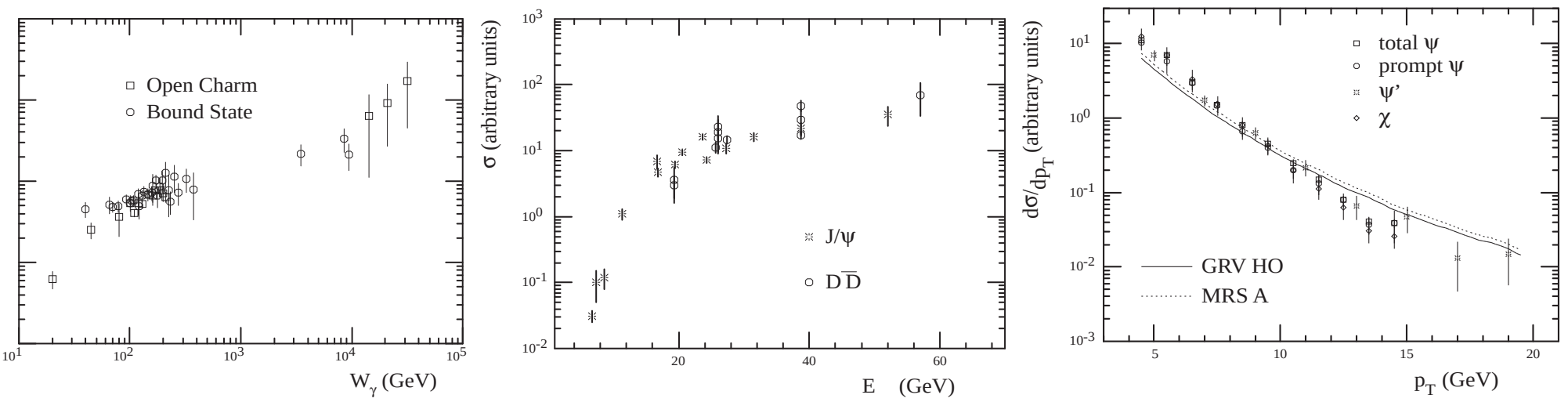

Figure 1: **(Left) Photoproduction data as a function of the photon energy in the hadron rest frame, W_γ. (Center) Hadroproduction data as a function of the center-of-mass energy, E_{cm}. In both cases, the normalization has been adjusted to show the similar shapes of the data. (Right) Run I data from the CDF Collaboration, shown with arbitrary normalization. The curves are the predictions of the color evaporation model at tree level, also shown with arbitrary normalization. [Amundson *et al.*]**

Choosing Parameters for J/ψ Calculations I: FONLL

J/ψ parameters based on FONLL parameter sets varying mass and scales around central value $(m, \mu_F/m, \mu_R/m) = (1.5\,\mathrm{GeV}, 1, 1)$ (left)

None of the FONLL sets fit the data

No convergence for $\mu_R/m < 1$ (large α_s)

Problems with backward evolution of PDFs for $\mu_F/m \leq 1$ (near or below minimum scale of PDFs)

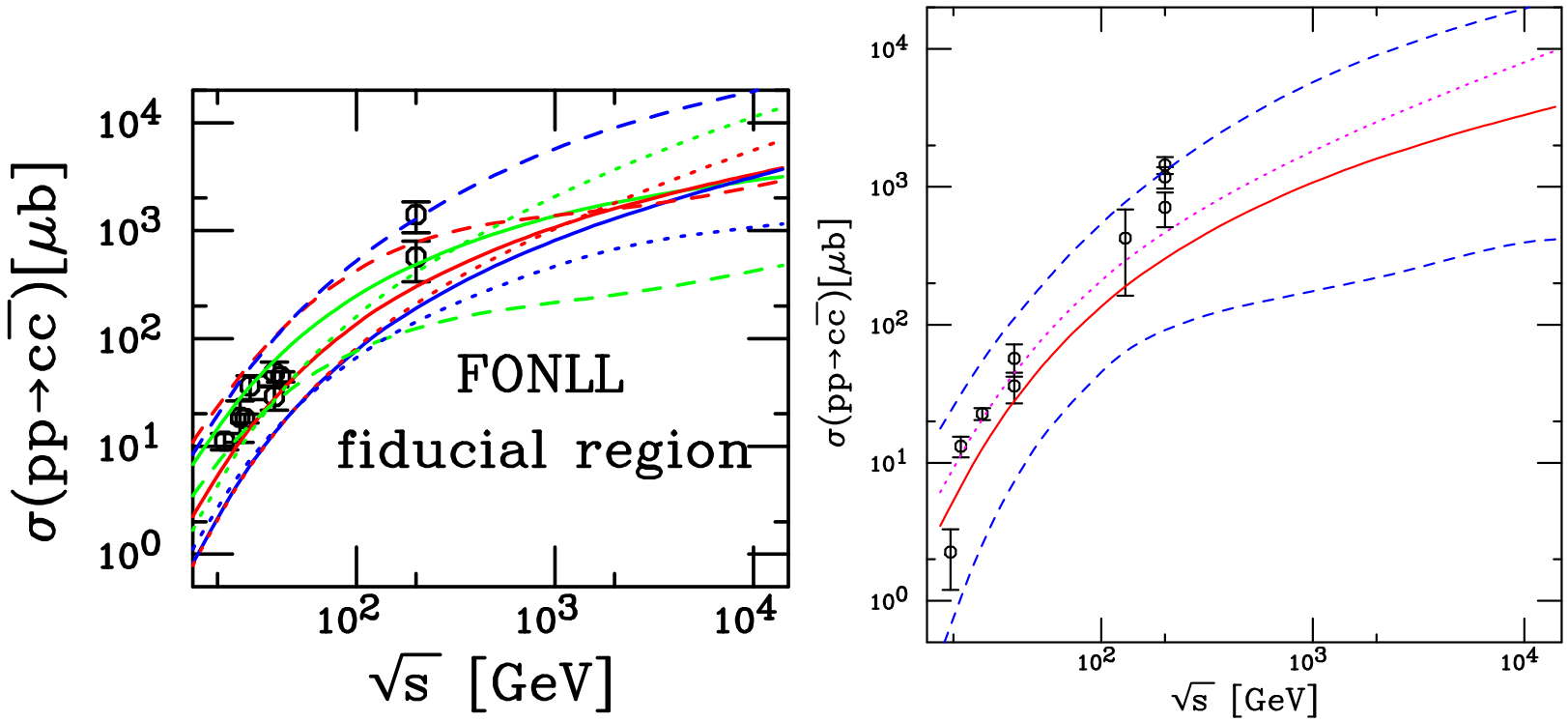

Figure 2: (Left) Total $c\bar{c}$ cross sections calculated using CTEQ6M. The solid red curve is the central value $(m, \mu_F/m, \mu_R/m) = (1.5\,\mathrm{GeV}, 1, 1)$. The green and blue solid curves are $(1.3\,\mathrm{GeV}, 1, 1)$ and $(1.7\,\mathrm{GeV}, 1, 1)$ respectively. The red, blue and green dashed curves correspond to $(1.5\,\mathrm{GeV}, 0.5, 0.5)$, $(1.5\,\mathrm{GeV}, 1, 0.5)$ and $(1.5\,\mathrm{GeV}, 0.5, 1)$ while the red, blue and green dotted curves are for $(1.5\,\mathrm{GeV}, 2, 2)$, $(1.5\,\mathrm{GeV}, 1, 2)$ and $(1.5\,\mathrm{GeV}, 2, 1)$. (Right) Uncertainty band formed from adding mass and scale uncertainties in quadrature.

Choosing Parameters for J/ψ Calculations II: Fitting $\sigma_{c\bar{c}}$

J/ψ parameters based on fits to NLO total $c\bar{c}$ cross section – caveat: K factors still factor ~ 2 (Kidonakis and RV)

Fix $\mu_F/m = 1, 2$ and let μ_R/m float; fit to fixed-target data (excludes RHIC data)

Even though χ^2 is the same as or smaller for $\mu_F/m = 1$ with similar μ_R/m, how does it behave at higher energies?

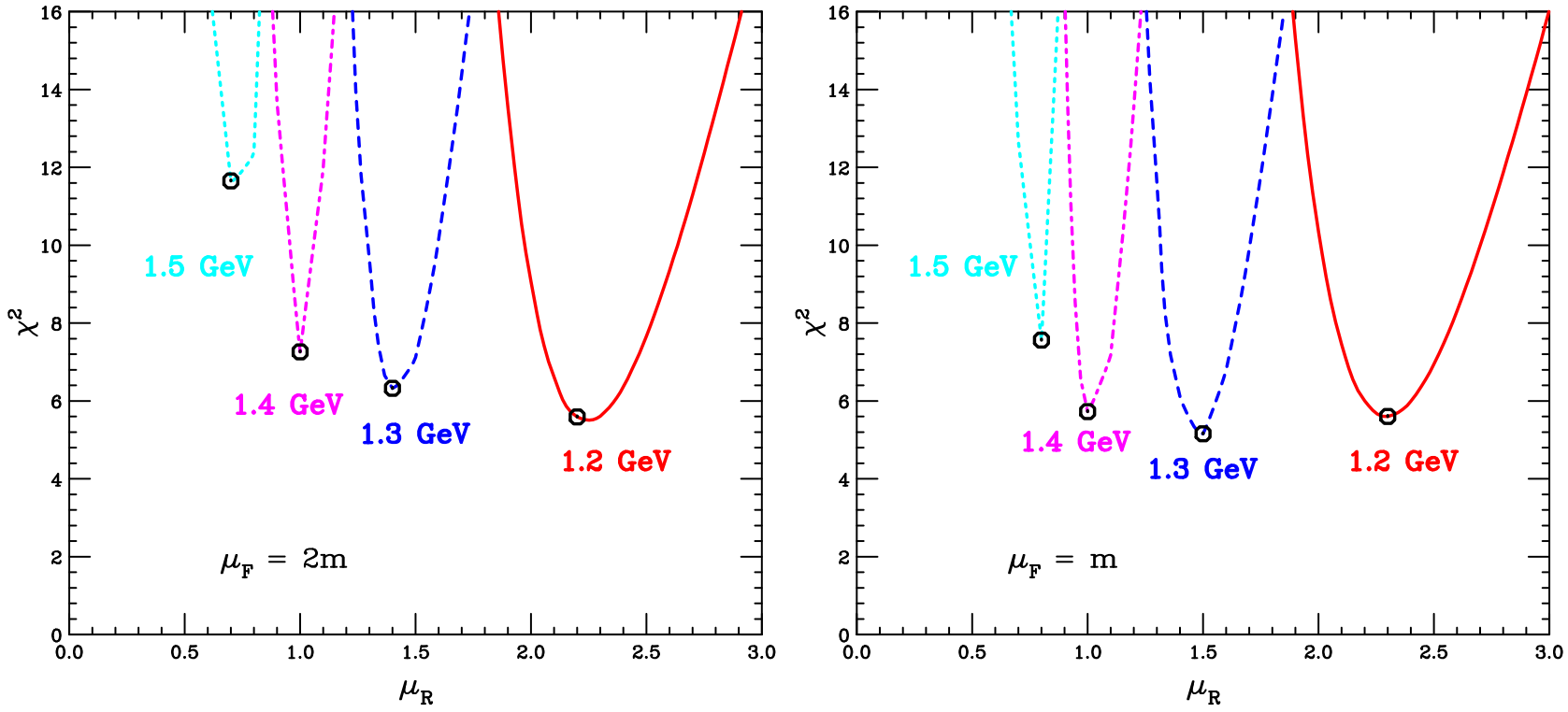

Figure 3: The calculated χ^2 for $\mu_F/m = 2$ (left) and 1 (right). The circles at the minimum of the curves on the left-hand side correspond to $(1.2\,\mathrm{GeV}, 2, 2.2)$, $(1.3\,\mathrm{GeV}, 2, 1.4)$, $(1.4\,\mathrm{GeV}, 2, 1)$, and $(1.5\mathrm{GeV}, 2, 0.7)$ while those on the right-hand side are with $(1.2\,\mathrm{GeV}, 1, 2.3)$, $(1.3\,\mathrm{GeV}, 1, 1.5)$, $(1.4\,\mathrm{GeV}, 1, 1)$, and $(1.5\mathrm{GeV}, 1, 0.8)$. The calculations are now done with the CT10 PDFs.

Choosing Parameters for J/ψ Calculations III: Best Fits?

Good agreement with fixed-target data does not guarantee good behavior at collider energies

$\mu_F/m = 2$ (left-hand side) gives more realistic result for collider energies than $\mu_F/m = 1$ (right-hand side), best energy dependence with 'worst' μ_R/m (0.8)

Low mass and higher μ_R/m flattens cross section for $\sqrt{s} \geq 40$ GeV

Use $(1.4\,\mathrm{GeV}, 2, 1)$ as 'central' value, $(1.2\,\mathrm{GeV}, 2, 2)$ and $(1.5\,\mathrm{GeV}, 2, 0.7)$ as lower and upper limits respectively

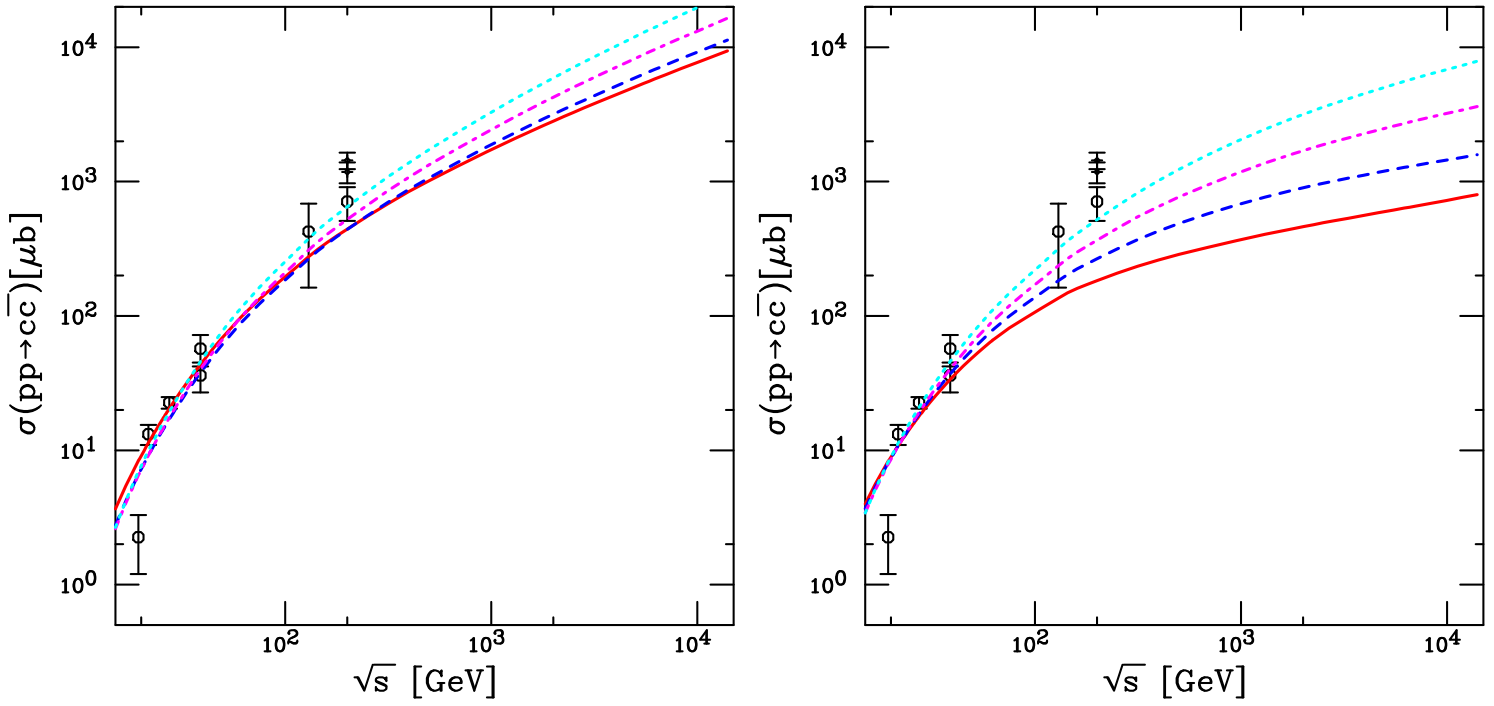

Figure 4: The calculated total $c\bar{c}$ cross sections for $\mu_F/m = 2$ (left) and 1 (right). The curves on the left-hand side are calculated with $(1.2\ \mathrm{GeV}, 2, 2)$ [solid red], $(1.3\ \mathrm{GeV}, 2, 1.4)$ [dashed blue], $(1.4\ \mathrm{GeV}, 2, 1)$ [dot-dashed magenta], and $(1.5\ \mathrm{GeV}, 2, 0.7)$ [dotted cyan] while those on the right-hand side are with $(1.2\ \mathrm{GeV}, 1, 2.5)$ [solid red], $(1.3\ \mathrm{GeV}, 1, 1.5)$ [dashed blue], $(1.4\ \mathrm{GeV}, 1, 1)$, [dot-dashed magenta] and $(1.5\ \mathrm{GeV}, 1, 0.8)$ [dotted cyan]. The calculations are now done with the CT10 PDFs.

J/ψ Cross Sections in CEM

From $\mu_F/m = 2$ fits, calculate J/ψ cross section to NLO in CEM, fit scale factor F_C

Energy dependence almost identical for all three parameter sets once mass cut is imposed (left-hand side)

Using normalization of 'central' result with $m = 1.4$ GeV for all sets gives minimal uncertainty band; now $(1.2\,\mathrm{GeV}, 2, 2)$ and $(1.5\,\mathrm{GeV}, 2, 0.7)$ are upper and lower limits

CTEQ6M and CT10 have nearly same value of F_C

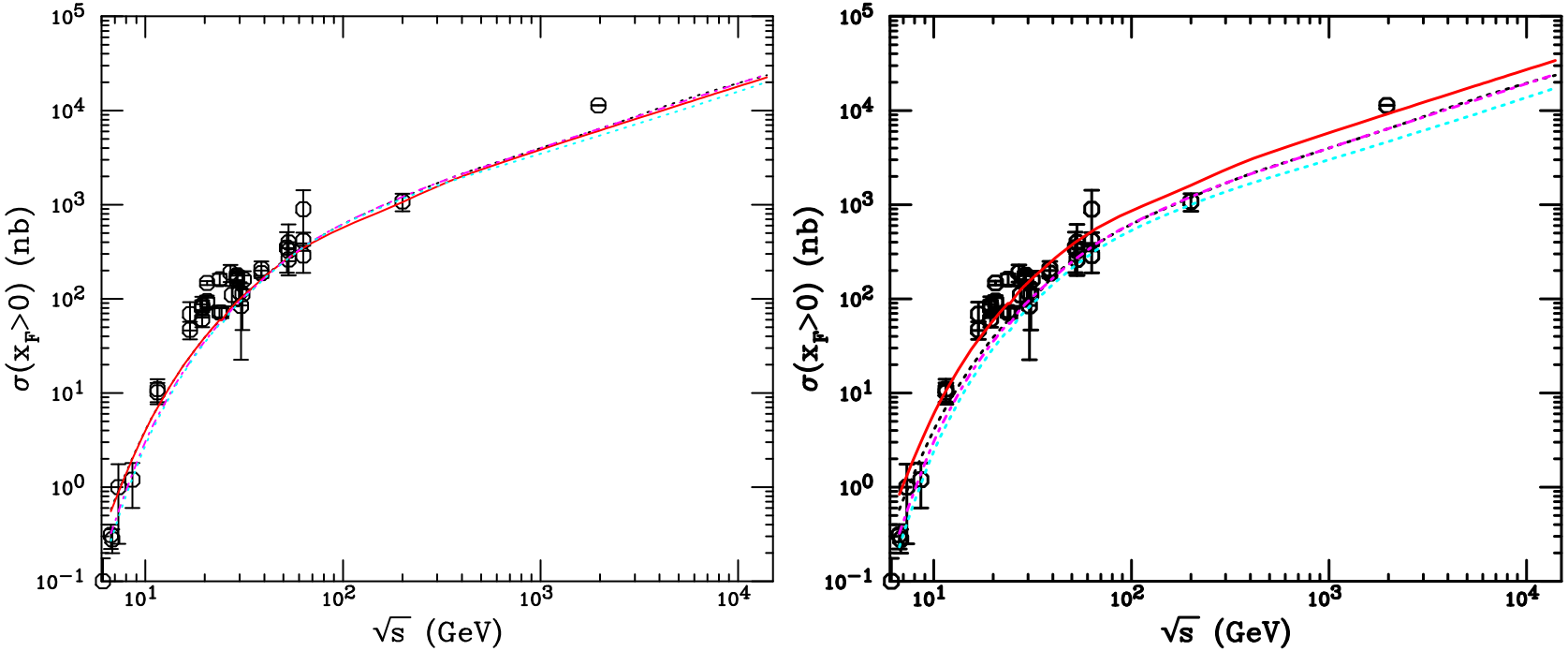

Figure 5: The calculated forward J/ψ cross sections. The curves are calculated with $(1.2\ \mathrm{GeV}, 2, 2)$ [solid red], $(1.4\ \mathrm{GeV}, 2, 1)$ [dot-dashed magenta], and $(1.5\ \mathrm{GeV}, 2, 0.7)$ [dotted cyan] using the CT10 PDFs. The results with CTEQ6M using $(1.2\ \mathrm{GeV}, 2, 2.2)$ [dotted black] are also shown. (Left-hand side) All curves are normalized using their fitted F_C. (Right-hand side) The new results are shown normalized to $(1.4\ \mathrm{GeV}, 2, 1)$.

Calculations of $b\bar{b}$ and Υ Better Behaved

Bottom quark mass is large enough for K factors to be smaller and $b\bar{b}$ cross section more reliable
FONLL mass and scale choices work well in this case

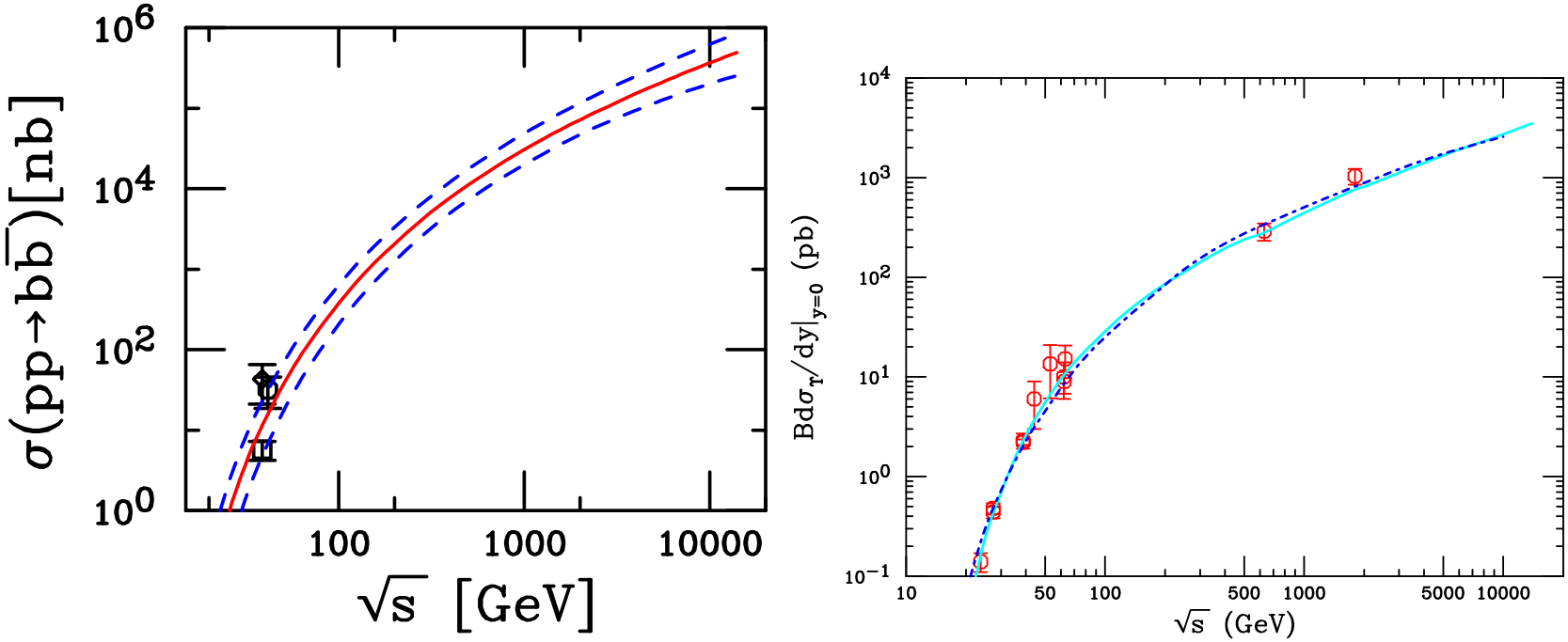

Figure 6: **The $b\bar{b}$ FONLL uncertainty band (left) and the combined Υ S states in the dilepton channel (right). Both are calculated to NLO in the CEM. [After Phys. Rept. 458 (2008) 1.]**

CEM p_T Distributions in the $Q\overline{Q}$ NLO Code

Without intrinsic k_T smearing (or resummation) the $Q\overline{Q}$ p_T distribution (LO at $\mathcal{O}(\alpha_s^3)$ while total cross section is NLO at this order) is too peaked at $p_T \to 0$, needs broadening at low p_T

Implemented by Gaussian k_T smearing, $\langle k_T^2 \rangle_p = 1$ GeV^2 for fixed target pp and πp, broadened for pA and AA, NLO code adds in final state:

$$g_p(k_T) = \frac{1}{\pi \langle k_T^2 \rangle_p} \exp(-k_T^2/\langle k_T^2 \rangle_p)$$

Broadening should increase with energy we make a simple linear extrapolation to obtain

$$\langle k_T^2 \rangle_p = 1 + \frac{1}{3n} \ln\left(\frac{\sqrt{s}}{\sqrt{s_0}}\right) \text{ GeV}^2$$

We find $n \sim 4$ agrees best with RHIC data

FONLL Employed to Calculate $B \to J/\psi X$

FONLL includes resummed terms (RS) of order $\alpha_s^2(\alpha_s \log(p_T/m))^k$ (leading log – LL) and $\alpha_s^3(\alpha_s \log(p_T/m))^k$ (NLL) while subtracting off fixed-order terms retaining only the "massless" limit of fixed order (FOM0)

FO calculation treats the heavy flavor ($n_f = 4$ for bottom) as heavy while the RS approach includes the heavy flavor as an active light degree of freedom ($n_f = 5$)

$$\text{FONLL} = \text{FO} + (\text{RS} - \text{FOM0})\ G(m, p_T)$$

At RHIC (Cacciari, Nason and RV) uncertainty band determined from mass range, $4.5 < m < 5$ GeV with $\mu_F = \mu_R = m$, and range of scales relative to central mass value, 4.75 GeV: $(\mu_F/m_T, \mu_R/m_T) = (1,1)$, (2,2), (0.5,0.5), (0.5,1), (1,0.5), (1,2), (2,1)

FONLL can calculate J/ψ contribution from inclusive B decays

$$\frac{E d^3\sigma(J/\psi)}{dp^3} = \frac{E_Q d^3\sigma(Q)}{dp_Q^3} \otimes D(Q \to H_Q) \otimes f(H_Q \to J/\psi)$$

Calculate uncertainty bands by adding upper and lower limits of mass and scale uncertainties in quadrature

$$\frac{d\sigma_{\max}}{dp_T} = \frac{d\sigma_{\text{cent}}}{dp_T} + \sqrt{\left(\frac{d\sigma_{\mu,\max}}{dp_T} - \frac{d\sigma_{\text{cent}}}{dp_T}\right)^2 + \left(\frac{d\sigma_{m,\max}}{dp_T} - \frac{d\sigma_{\text{cent}}}{dp_T}\right)^2}$$

$$\frac{d\sigma_{\min}}{dp_T} = \frac{d\sigma_{\text{cent}}}{dp_T} - \sqrt{\left(\frac{d\sigma_{\mu,\min}}{dp_T} - \frac{d\sigma_{\text{cent}}}{dp_T}\right)^2 + \left(\frac{d\sigma_{m,\min}}{dp_T} - \frac{d\sigma_{\text{cent}}}{dp_T}\right)^2}$$

CEM Comparison to RHIC pp J/ψ Data

CEM calculation reproduces shape of J/ψ p_T and y distributions rather well

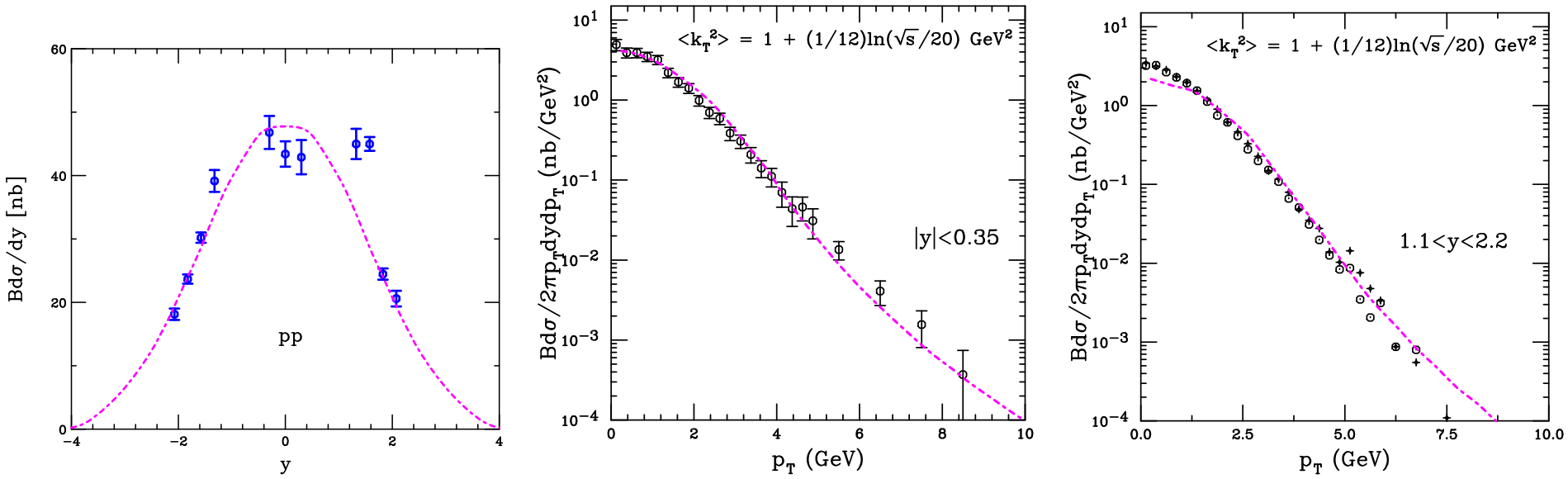

Figure 7: **PHENIX pp measurements compared to CEM calculation at $\sqrt{s} = 200$ GeV. The J/ψ rapidity distribution (left) and transverse momentum distributions at midrapidity (center) and in the muon arms (right). The results are calculated with CTEQ6M, $(m, \mu_F/m_T, \mu_R/m_T) = (1.2, 2, 2)$, $\langle k_T^2 \rangle = 1.38$ GeV^2. The forward result is scaled up by a factor of ≈ 1.4.**

CEM Comparison to LHC pp Quarkonium Data

CEM calculation reproduces shape of J/ψ and $\Upsilon(1S)$ p_T distributions using CTEQ6M with $(m, \mu_F/m_T, \mu_R/m_T) = (1.2\ \text{GeV}, 2, 2)$, $\langle k_T^2 \rangle = 1.38\ \text{GeV}^2$.
No 'fudge' factor included

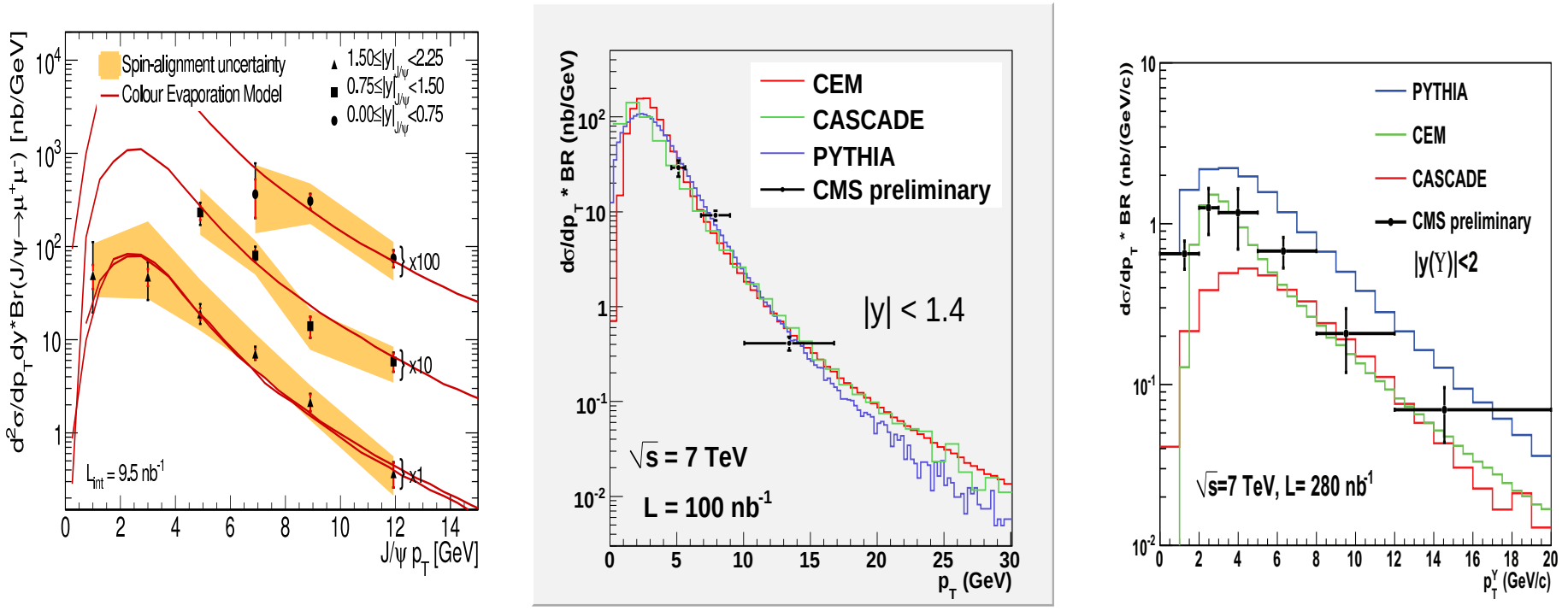

Figure 8: **ATLAS (left) and CMS (middle) J/ψ and CMS $\Upsilon(1S)$ (right) cross sections at 7 TeV compared to CEM calculations.**

CEM Uncertainty Using $c\bar{c}$ Fits

Curves do not differ substantially at higher p_T, only at low p_T

Factor of several in total $c\bar{c}$ cross section does not lead to large J/ψ uncertainty

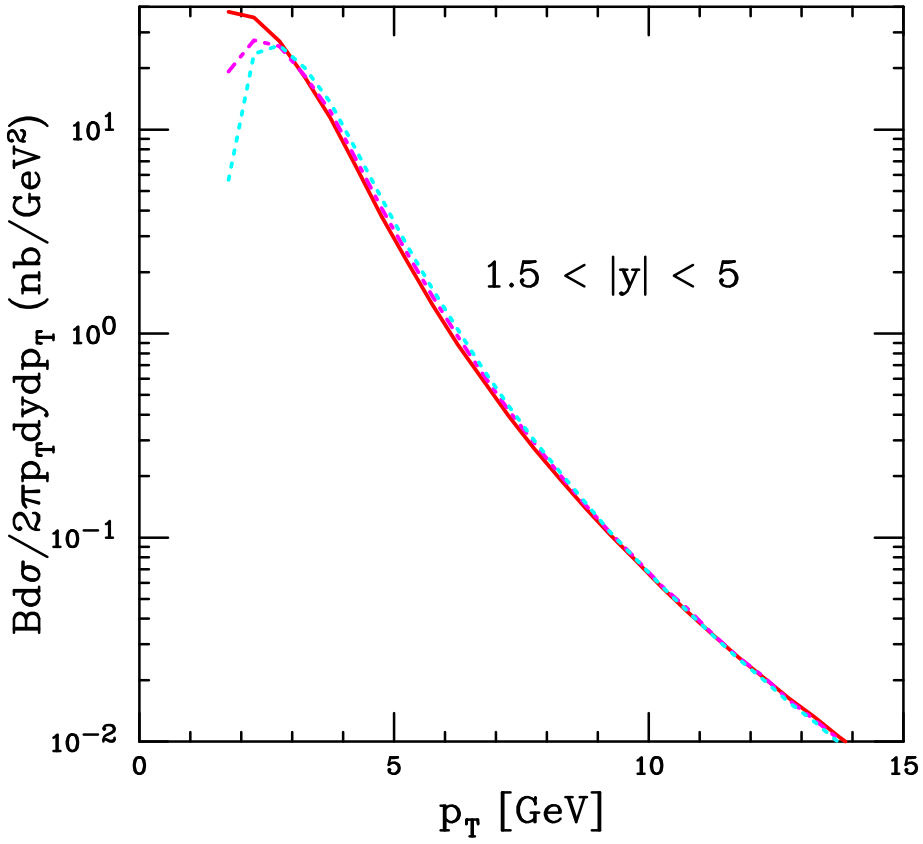

Figure 9: **LHCb J/ψ uncertainty using** $(1.2\ \text{GeV}, 2, 2)$ **[solid red],** $(1.4\ \text{GeV}, 2, 1)$ **[dot-dashed magenta], and** $(1.5\ \text{GeV}, 2, 0.7)$ **[dotted cyan] in the rapidity interval** $1.5 < |y| < 5$**. All curves share the 1.4 GeV normalization.**

Calculation of J/ψ Contribution from B decays

B production calculated using FONLL, uncertainty comes from varying the mass and scale around central value of $(4.75\,\mathrm{GeV}, 1, 1)$ and adding uncertainties in quadrature

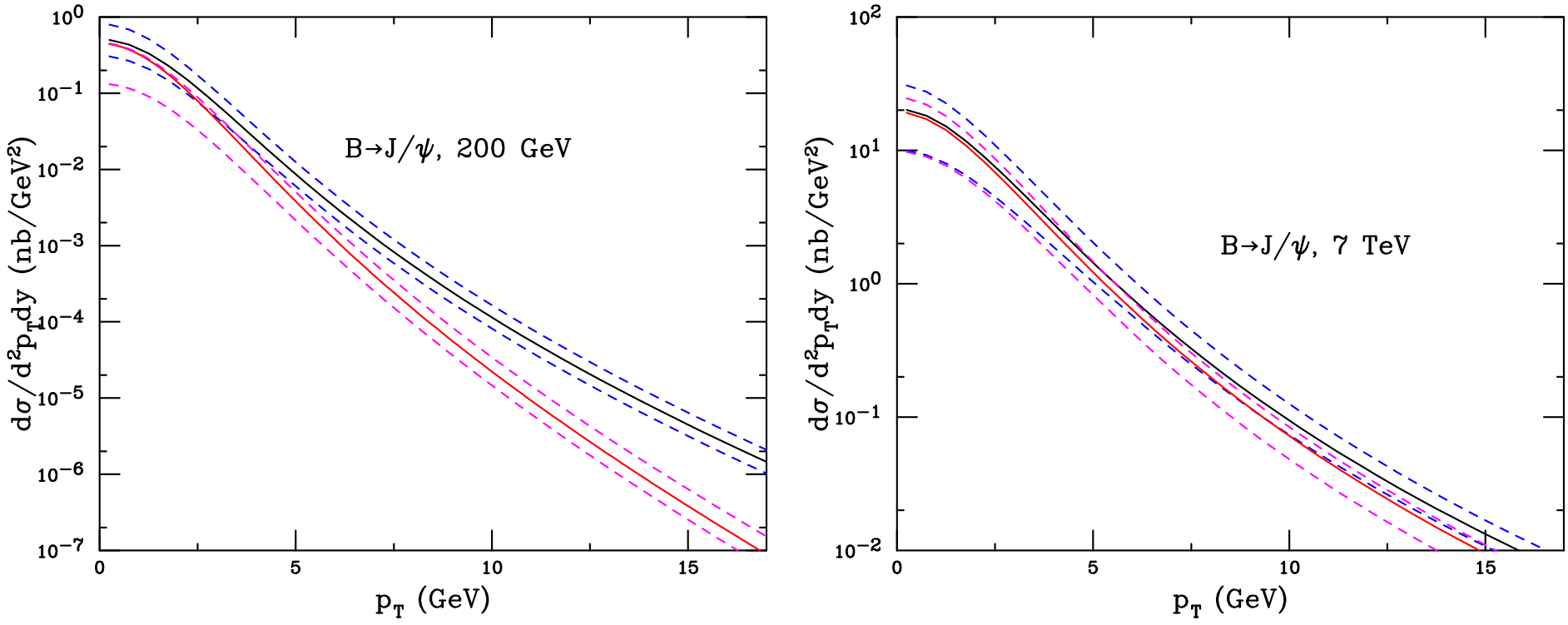

Figure 10: **Calculation of the invariant p_T distribution for B decay to J/ψ in pp collisions at $\sqrt{s} = 200$ GeV (left) and 7 TeV (right) from FONLL. The two rapidity bins for 200 GeV are $0.35 < |y|$ (black and blue) and $1.1 < |y| < 2.2$ (red and magenta) while the two bins for 7 TeV are $1.4 < |y|$ (black and blue) and $1.4 < |y| < 2.4$ (red and magenta).**

Fraction of J/ψ from B Decays at 200 GeV

$$B\,\text{fraction} \equiv \frac{B \to J/\psi X}{\text{prompt, inclusive}\, J/\psi + B \to J/\psi X}$$

Prompt inclusive J/ψ calculated in CEM, band is from uncertainty on B cross section only

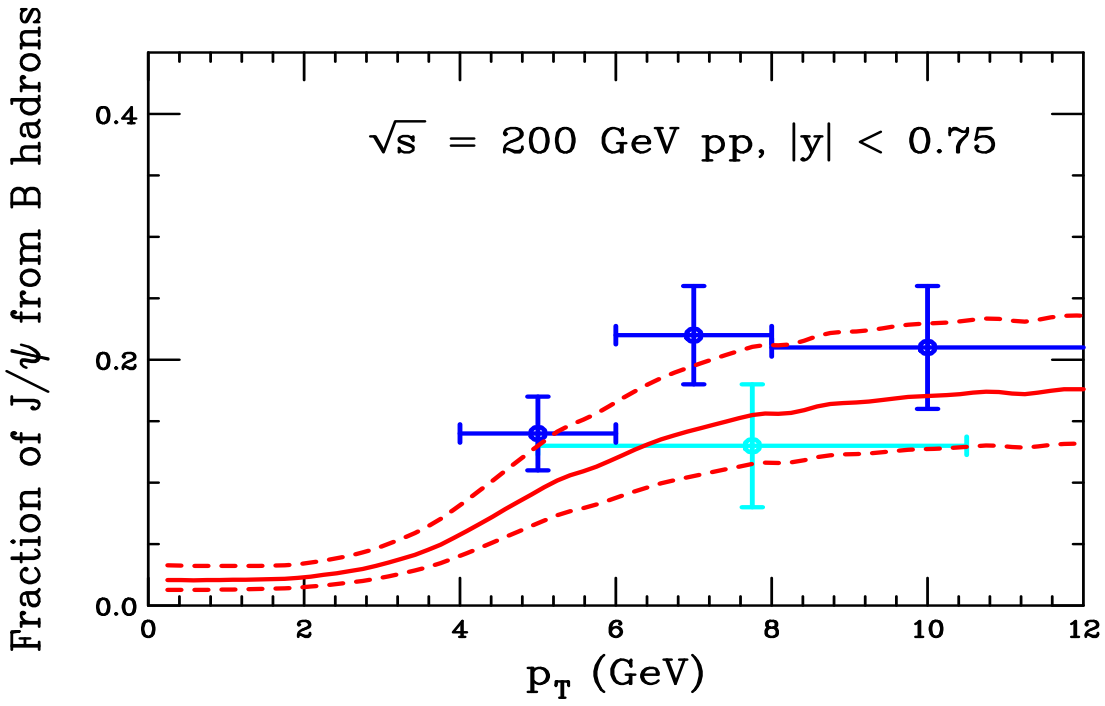

Figure 11: The fraction of J/ψ production from B decays as a function of p_T.

$B \to J/\psi$ Fraction at Tevatron and LHC

Good agreement with preliminary LHC pp data at 7 TeV

CDF $\overline{p}p$ data at 1.96 TeV has somewhat different curvature but only disagrees with calculated ratio for $p_T > 15$ GeV

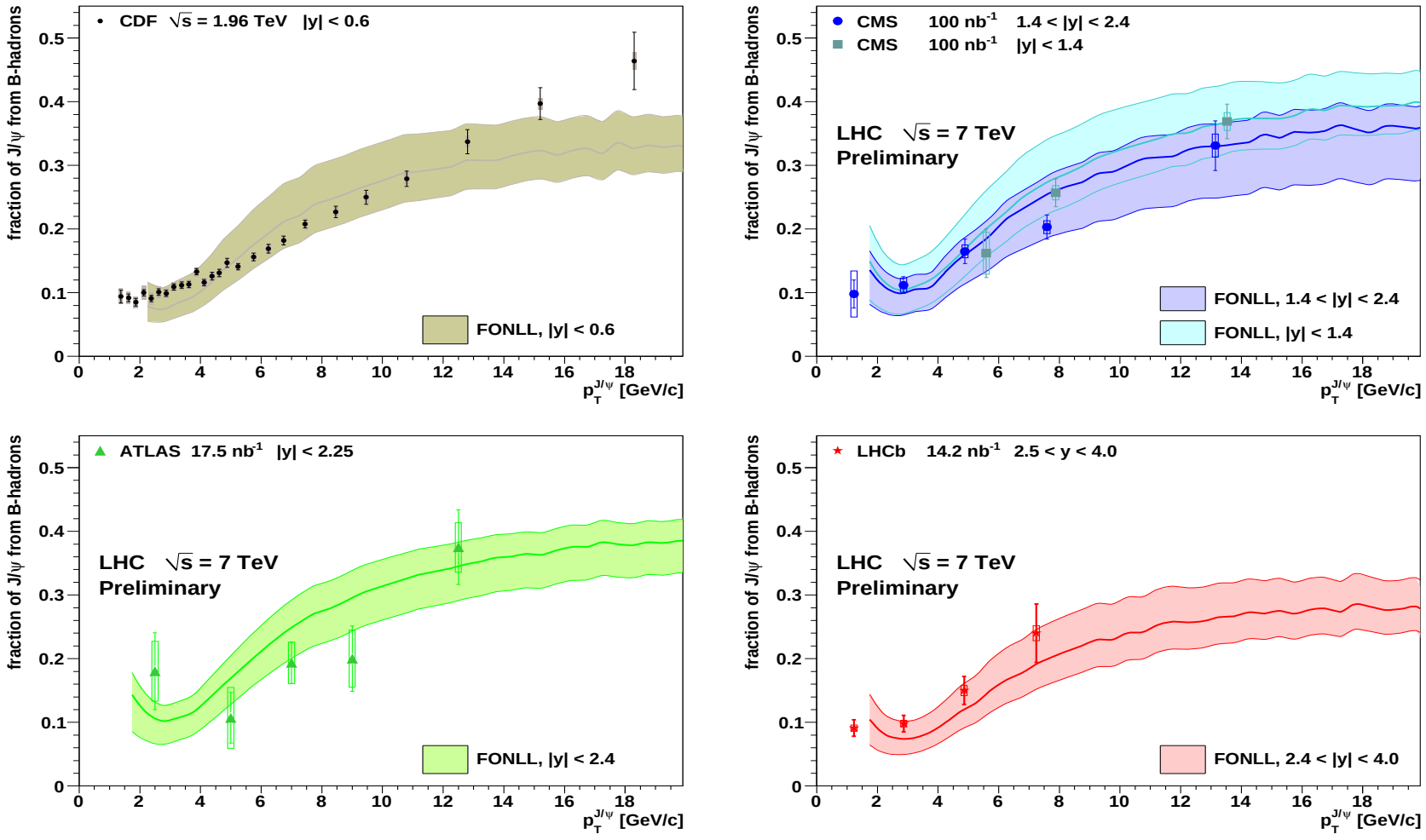

Figure 12: **The fraction of J/ψ from B decays at 1.96 TeV (CDF) and 7 TeV (CMS, ATLAS and LHCb).**

pA and dA Production

What Are Cold Matter Effects?

Important cold nuclear matter effects include:

- **Initial-state nuclear effects on the parton densities (shadowing)**
- **Initial-state energy loss**
- **Intrinsic heavy flavors**
- **Final-state absorption on nucleons**

Shadowing and absorption most important at midrapidity, initial-state energy loss and intrinsic heavy flavor more important at forward rapidity

Production mechanism affects both intimately:

- **Shadowing depends on momentum fraction x of the target (and projectile in AA) which is influenced by how the state was produced: $2 \to 1$ or $2 \to 2$ process**
- **Production affects absorption because singlet and octet states can be absorbed differently**

Medium Effects Important in p(d)+A Interactions

Nuclear effects in fixed-target interactions

Parameterizing

$$\sigma_{pA} = \sigma_{pp} A^{\alpha} \qquad \alpha(x_F, p_T)$$

For $\sqrt{s_{NN}} \leq 40$ GeV and $x_F > 0.25$, α decreases strongly with x_F – only low x_F effects probed by SPS and RHIC rapidity coverage

Consider two low x_F cold matter effects at colliders:

- **Nuclear Shadowing (nPDFs) — initial-state effect on the parton distributions affecting total rate, important as a function of y/x_F**
- **Absorption — final-state effect, after $c\overline{c}$ that forms the J/ψ has been produced, pair breaks up in matter due to interactions with nucleons**

At high x_F/y, other mechanisms (energy loss, intrinsic charm) may be important, to be discussed later

Effects of nPDFs at LO and NLO

While the magnitude of the absolute cross sections may differ at LO and NLO, the effect of shadowing is, by design, the same at LO and NLO

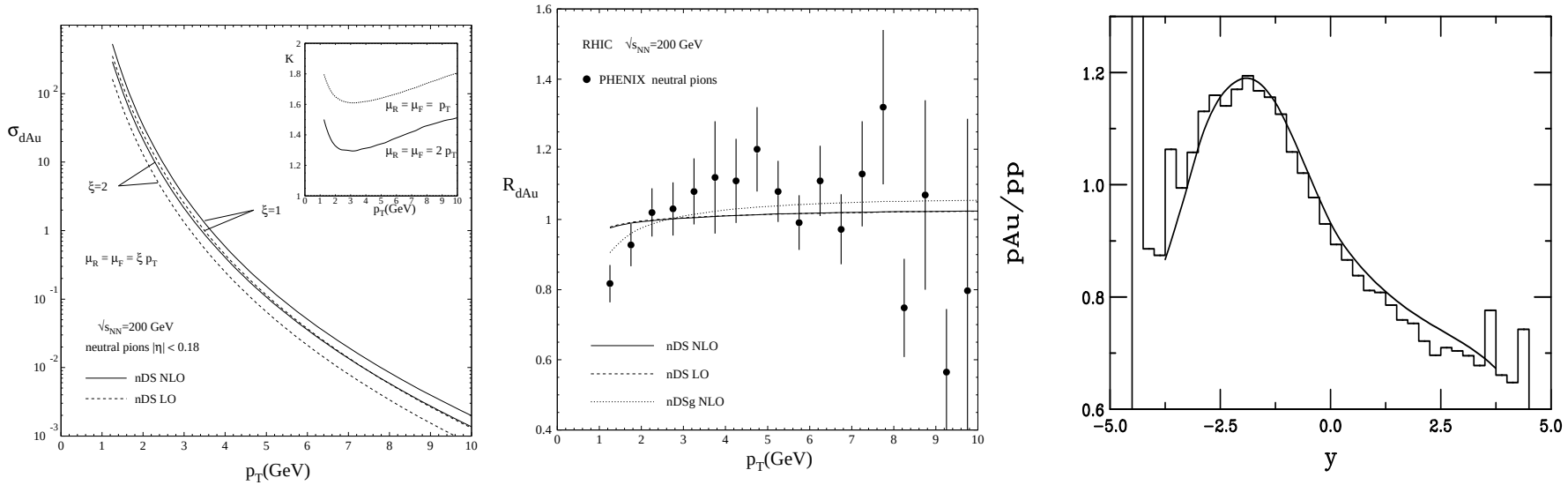

Figure 13: **Left: The π^0 cross section in d+Au collisions at $\sqrt{s_{NN}} = 200$ GeV at LO and NLO. Center: The LO and NLO calculations of $R_{\rm dAu}$ for π^0 production. Right: The J/ψ $R_{\rm dAu}$ as a function of rapidity at $\sqrt{s_{_{NN}}} = 200$ GeV at LO (curve) and NLO (histogram).**

Comparing Shadowing Parameterizations

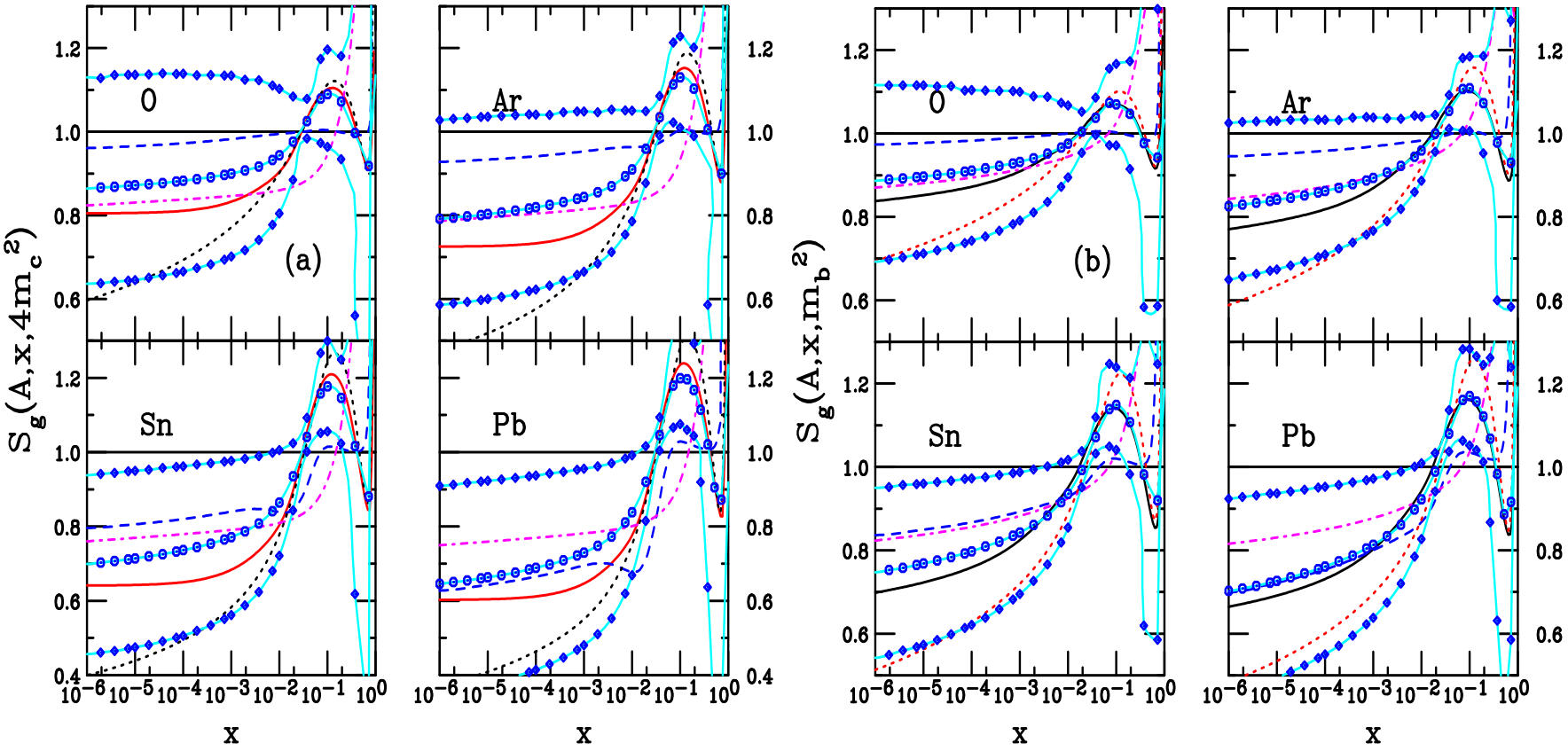

Figure 14: **Comparison of EKS98 (red), nDSg (blue), HKN (green), EPS08 (magenta), and EPS09 (cyan, with symbols) gluon shadowing parameterizations for J/ψ (left) and Υ (right) production scales with A =O, Ar, Sn and Pb.**

Quarkonium Absorption by Nucleons

Woods-Saxon nuclear density profiles typically used

$$\begin{aligned}\sigma_{pA} &= \sigma_{pN}\int d^2b \int_{-\infty}^{\infty} dz\, \rho_A(b,z) S_A^{\rm abs}(b) \\ &= \sigma_{pN}\int d^2b \int_{-\infty}^{\infty} dz\, \rho_A(b,z) \exp\left\{-\int_z^{\infty} dz' \rho_A(b,z')\sigma_{\rm abs}(z'-z)\right\}\end{aligned}$$

Note that if $\rho_A = \rho_0$, $\alpha = 1 - 9\sigma_{\rm abs}/(16\pi r_0^2)$

The value of $\sigma_{\rm abs}$ **depends on the parameterization of** σ_{pA} **– Glauber, hard sphere,** A^α **etc. (shown by NA50)**

Initial-state shadowing, only recently taken into account at SPS energies

Feed down to J/ψ **from** χ_c **and** ψ' **decays not always included, should dictate that**

$$\sigma_{pA} = \sigma_{pN}\int d^2b\, [0.6 S_{\psi,\,\rm dir}(b) + 0.3 S_{\chi_{cJ}}(b) + 0.1 S_{\psi'}(b)]$$

Assume that each charmonium state interacts with a different constant asymptotic absorption cross section

The χ_c A **dependence remains unknown**

A Dependence of J/ψ and ψ' Not Identical: Size Matters

Color octet mechanism suggested that J/ψ and ψ' A dependence should be identical — Supported by large uncertainties of early data

More extensive data sets (NA50 at SPS, E866 at FNAL) show clear difference at midrapidity [NA50 ρL fit gives $\Delta\sigma = \sigma^{\psi'}_{\rm abs} - \sigma^{J/\psi}_{\rm abs} = 4.2 \pm 1.0$ mb at 400 GeV, 2.8 ± 0.5 mb at 450 GeV for absolute cross sections]

Suggests we need to include formation time effects

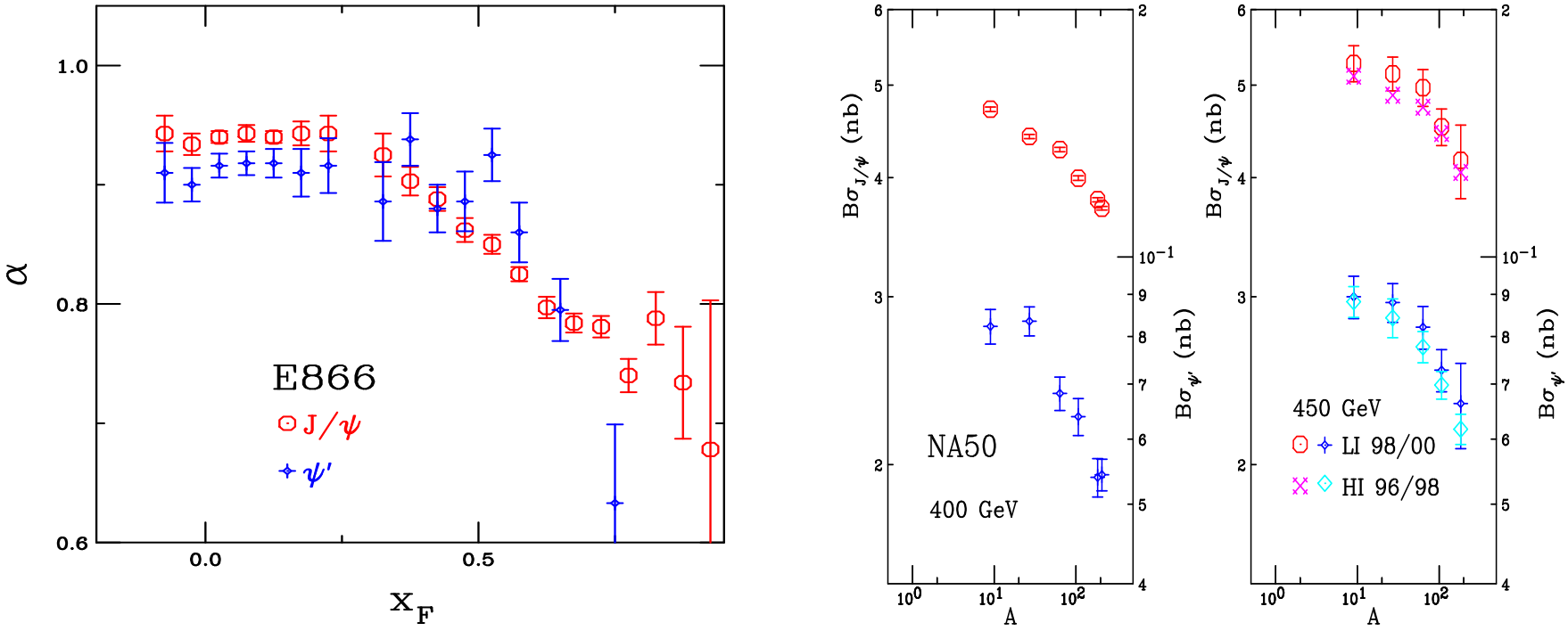

Figure 15: **The J/ψ A dependence (left) as a function of x_F at FNAL ($\sqrt{s_{NN}} = 38.8$ GeV) and (right) and a function of A at the SPS (NA50 at $p_{\rm lab} = 400$ and 450 GeV) for J/ψ and ψ' production.**

Energy Dependence of $\sigma_{\rm abs}^{J/\psi}$

At midrapidity, there seems to be a systematic decrease of the absorption cross section with energy independent of shadowing

$\sigma_{\rm abs}^{J/\psi}(y_{\rm cms}=0)$ extrapolated to 158 GeV is significantly larger than measured at 450 GeV, underestimating "normal nuclear absorption" in SPS heavy-ion data

Calculations confirmed by NA60 pA measurements at 158 GeV (QM09)

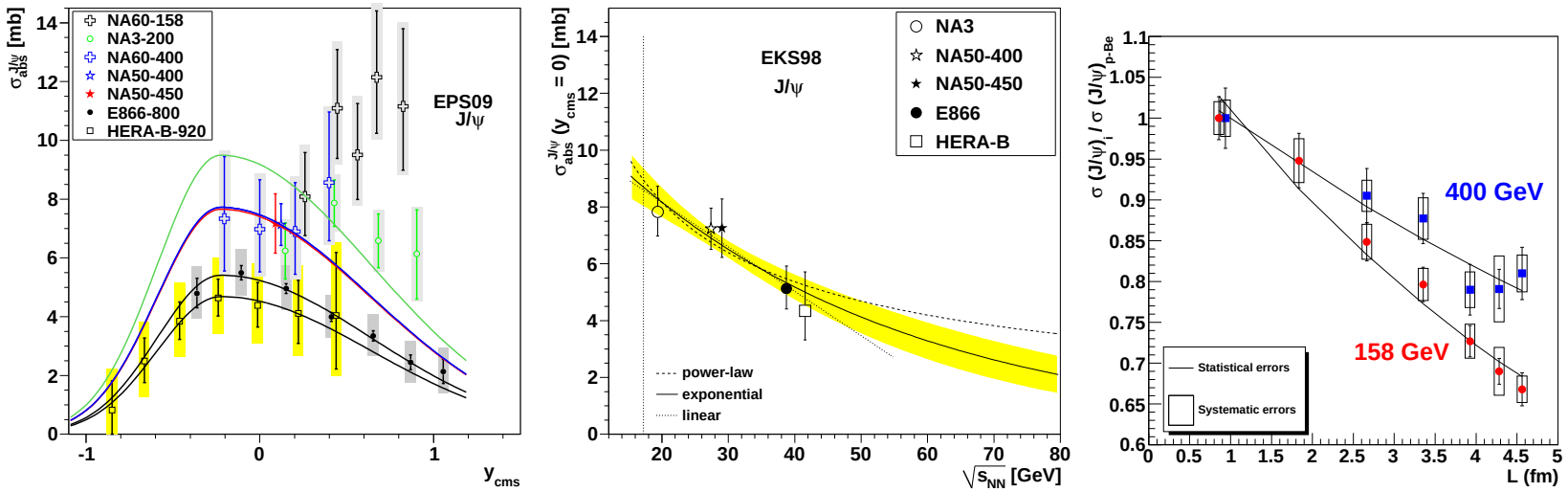

Figure 16: Left: Dependence of $\sigma_{\rm abs}^{J/\psi}$ on $y_{\rm cms}$ for all available data sets including EPS09 shadowing. The shape of the curves is fixed by the E866 and HERA-B data. [Lourenço, RV, Wöhri] Middle: The extracted energy dependence of $\sigma_{\rm abs}^{J/\psi}$ at midrapidity for power law (dashed), exponential (solid) and linear (dotted) approximations to $\sigma_{\rm abs}^{J/\psi}(y=0,\sqrt{s_{NN}})$ using the EKS98 shadowing parameterization with the CTEQ61L parton densities. The band around the exponential curve indicates the uncertainty in the extracted cross sections at $x_F \sim 0$ from NA3, NA50 at 400 and 450 GeV, E866 and HERA-B. The vertical dotted line indicates the energy of the Pb+Pb and In+In collisions at the CERN SPS. [Lourenço, RV, Wöhri] Right: The J/ψ cross section ratios for pA collisions at 158 GeV (circles) and 400 GeV (squares), as a function of L, the mean thickness of nuclear matter traversed by the J/ψ. [Arnaldi, Cortese, Scomparin]

$\sigma_{\rm abs}^{J/\psi}(y_{\rm cms})$ Rises at Forward Rapidity

Forward x_F ($y_{\rm cms}$) data more complex: strongly increased absorption in this region

NA60 data begin to rise at lower x_F than do higher energy results from E866 and PHENIX R_{CP} data: CGC?!?, not low enough x

Such strong effects can't come from any shadowing parameterizations

CSM results give smaller $\sigma_{\rm abs}$ (red, right) but exhibit same rise at larger $y_{\rm cms}$

Energy loss??? Or something else???

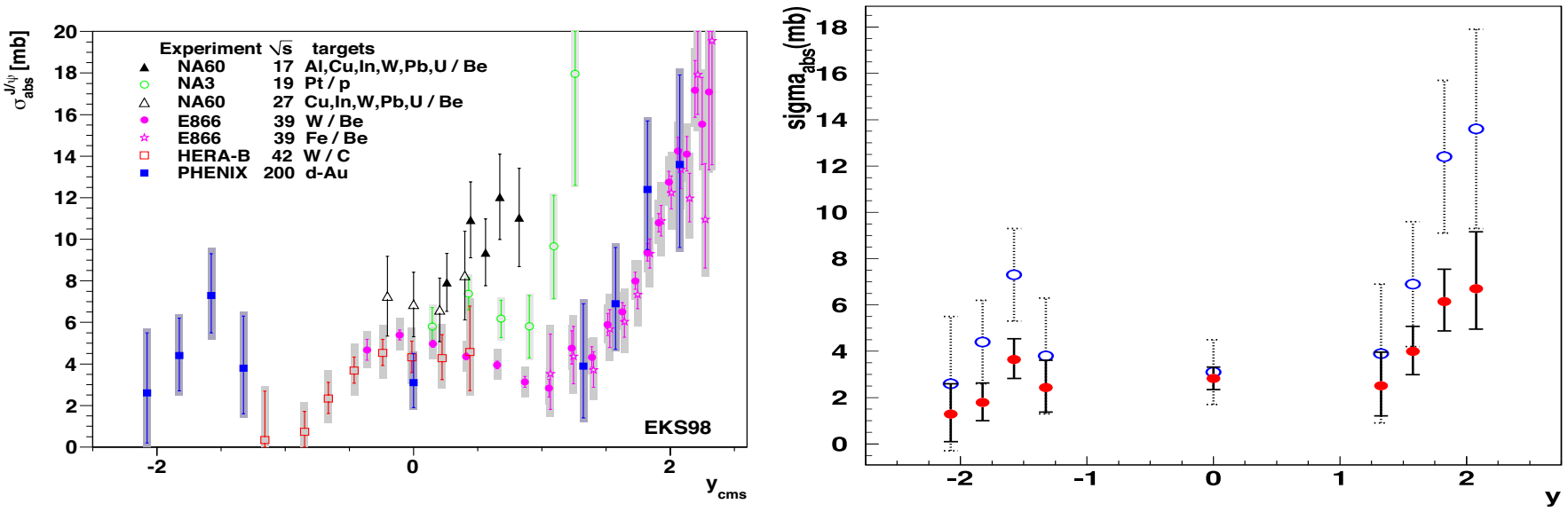

Figure 17: Left: The center-of-mass rapidity dependence of $\sigma_{\rm abs}^{J/\psi}$ for incident fixed-target energies from 158, 200, 400, 450, 800, 920 GeV and preliminary PHENIX results from RHIC obtained using the EKS98 shadowing parameterization. (Plot made by Hermine Wöhri with PHENIX data from Tony Frawley.) Right: Comparison of PHENIX results using CEM with CSM (Ferreiro *et al.*).

Is It Strong Energy Loss or Inhomogeneous Shadowing?

Most recent RHIC minimum bias (impact-parameter integrated shadowing) d+Au data agrees with EPS09 shadowing and 4 mb absorption cross section

The R_{CP} ratio does not agree with the impact-parameter dependent shadowing calculation at forward rapidity because the peripheral result is overestimated

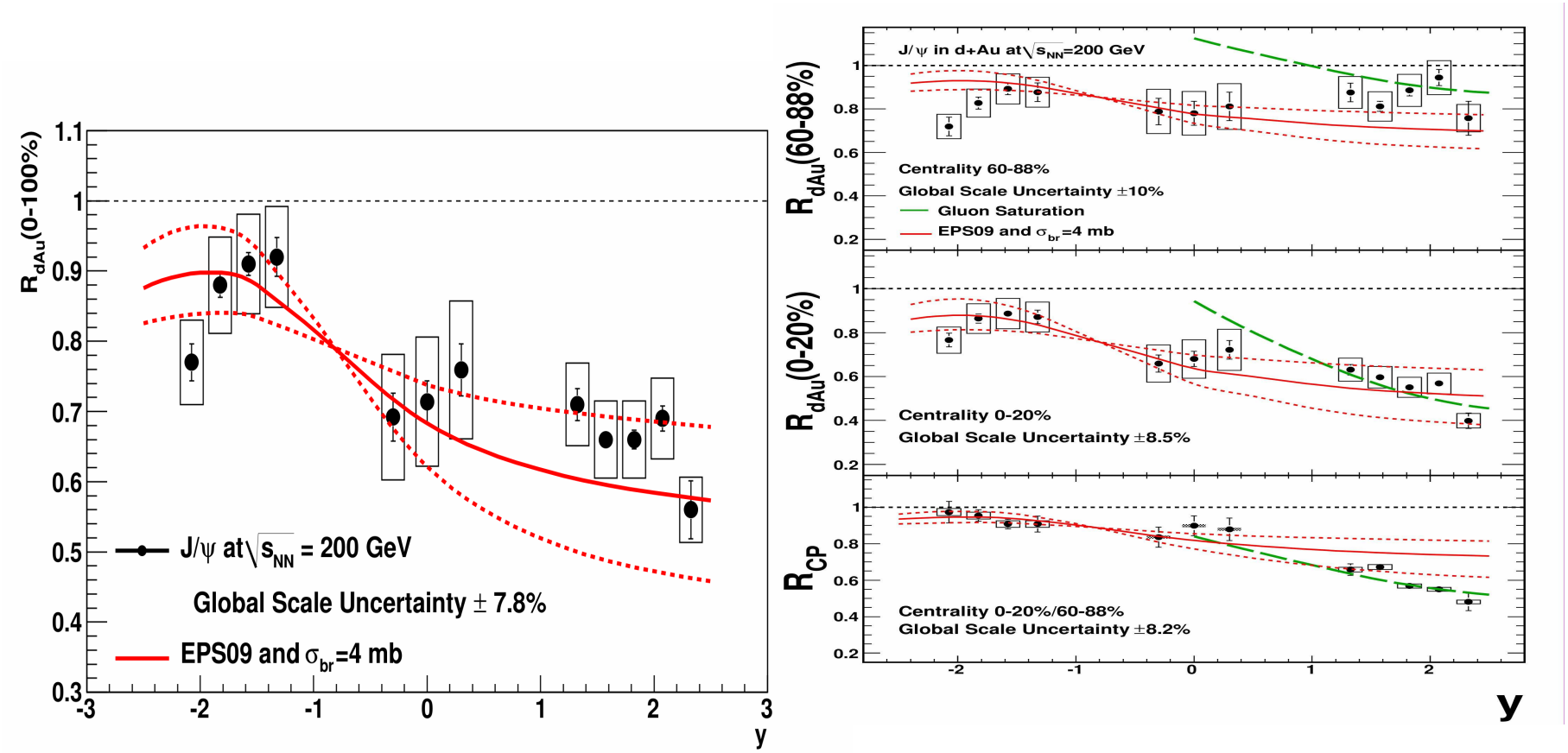

Figure 18: The PHENIX data compared to calculations of EPS09 shadowing including uncertainties and a constant absorption cross section of 4 mb. Left: the minimum bias result. Right: Including impact-parameter dependent shadowing in the $60-88\%$ centrality (top) and $0-20\%$ centrality (middle) bins. The lower panel shows the central-to-peripheral ratio. The dashed curves shows a gluon saturation calculation.

Nuclear Parton Distributions

Nuclear parton densities

$$\begin{aligned} F_i^A(x,Q^2,\vec{r},z) &= \rho_A(s) S^i(A,x,Q^2,\vec{r},z) f_i^N(x,Q^2) \\ s &= \sqrt{r^2+z^2} \\ \rho_A(s) &= \rho_0 \frac{1+\omega(s/R_A)^2}{1+\exp[(s-R_A)/d]} \end{aligned}$$

With no nuclear modifications, $S^i(A,x,Q^2,\vec{r},z) \equiv 1$

Assume spatial dependence proportional to a power of nuclear path length:

$$S^i_\rho(A,x,Q^2,\vec{r},z) = 1 + N_\rho(S^i(A,x,Q^2)-1)\Big(\frac{\int dz \rho_A(\vec{r},z)}{\int dz \rho_A(0,z)}\Big)^n$$

Alternatively, assume spatial dependence proportional to power of nuclear density:

$$S^i_{\rm WS}(A,x,Q^2,\vec{r},z) = 1 + N_{\rm WS}(S^i(A,x,Q^2)-1)\Big(\frac{\rho_A(\vec{r},z)}{\rho_A(0,z)}\Big)^n$$

Density-dependent parameteriation has sharper transition from shadowing to no shadowing as a function of impact parameter

Deutron density uses Hulthen wavefunction to calculate density

Normalization: $(1/A)\int d^2r dz \rho_A(s) S^i_\rho \equiv S^i$**. Larger than average modifications for** $s=0$**. Nucleons like free protons when** $s \gg R_A$**.**

Changing Impact Parameter Dependence of Shadowing

Assuming normal deuteron density with path length dependence gives rather slow change with b, increasing the power of the path length increases the central value and makes $S_{\mathrm{d}A}(b) \to 1$ faster

Assuming path length dependence with pA interactions instead of dA (only one nucleon in deuteron interacts) deepens and sharpens b dependence

Assuming density dependence in pA does not deepen density dependence as much but $S_{pA} \to 1$ at higher b

All results shown for $y = 2$, similar at other rapidities

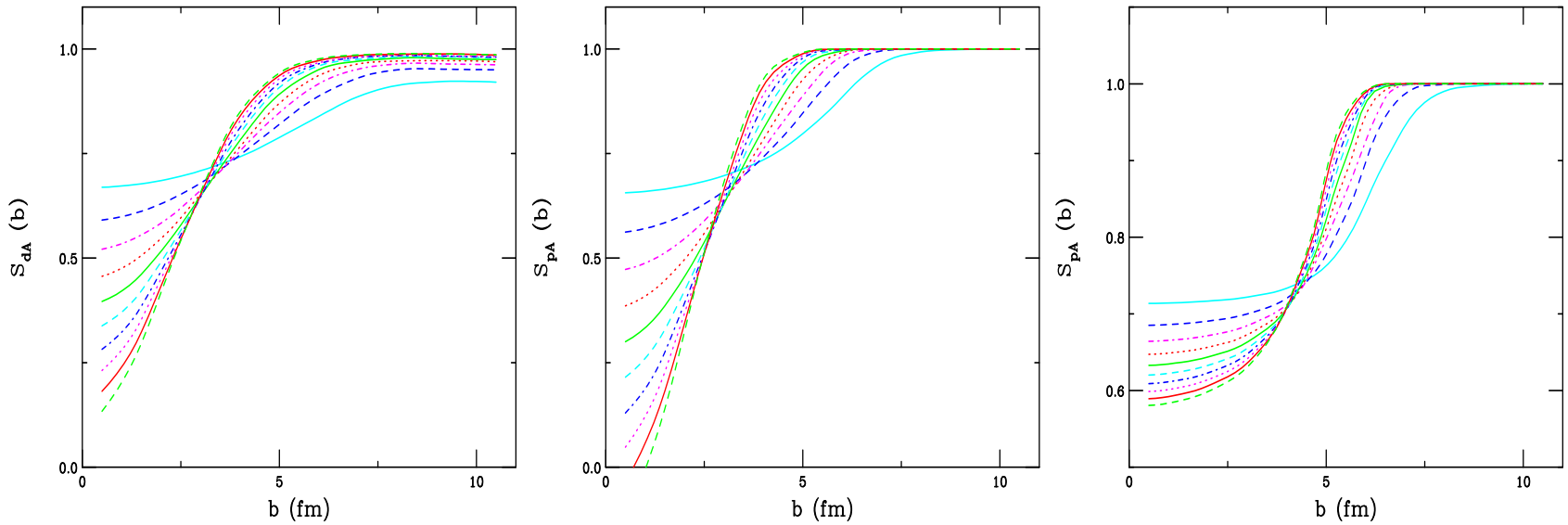

Figure 19: Changing the power of shadowing b-dependence from $n = 1$ (solid cyan) to 10 (dashed green) for dA collisions (left) and pA collisions (middle) with the path-length dependence and pA collisions with local density dependence (right). All calculations are at $y = 2$.

Drell-Yan Production: Testing Ground for Energy Loss

Good theory for pp production, small K factor with NLO calculation

$K = 1.124 \pm 0.007$, $\chi^2/\mathrm{ndf} = 1.4$ relative to E866 measurements in 800 GeV pp collisions (J.C. Webb Ph.D. thesis [arXiv:hep-ex/0302019]).

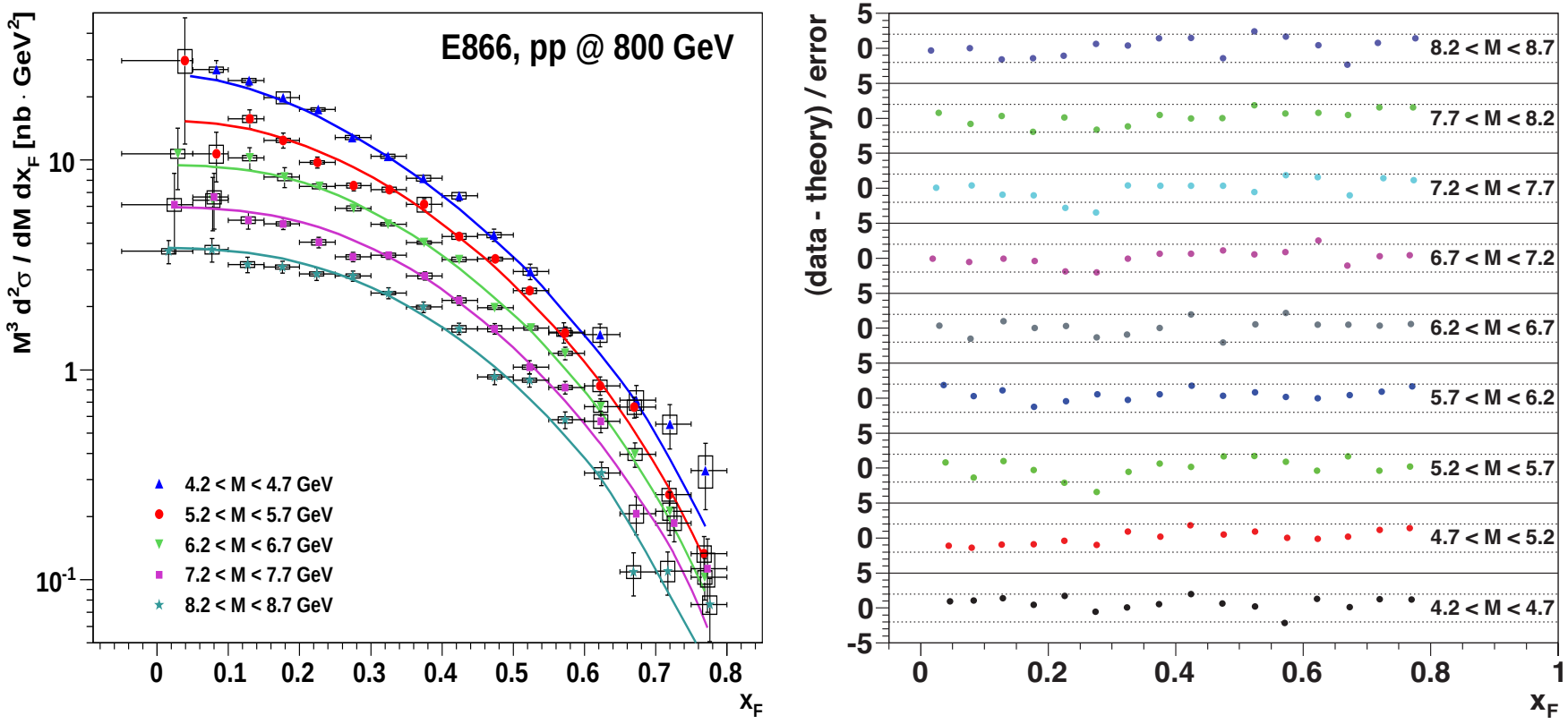

Figure 20: Left: The x_F dependence of the Drell-Yan cross section in several mass bins from 800 GeV pp colisions compared to NLO calculations. Right: Difference between the measured Drell-Yan cross section and the NLO calculations in the same mass bin.

Test Case: NA3 pPt Drell-Yan Production at 400 GeV

Compare NA3 data with NLO calculations with/without central EPS09 nPDFs (difference small)

Test parameterization of initial state energy loss

$$x_1' = x_1(1-\epsilon_q)^{N-1}$$

x_1' enters $M^2 = x_1' x_2 s_{_{NN}}$, x_1 is in nPDFs, N is number of NN collisions, $\propto A^{1/3}$

Vary ϵ_q to get best fit, 99% confidence level gives upper limit on ϵ_q of 0.0020

Assume $\epsilon_g = (9/4)\epsilon_q$ for NLO qg contribution

$K \sim 1$, χ^2/ndf slightly smaller with no shadowing

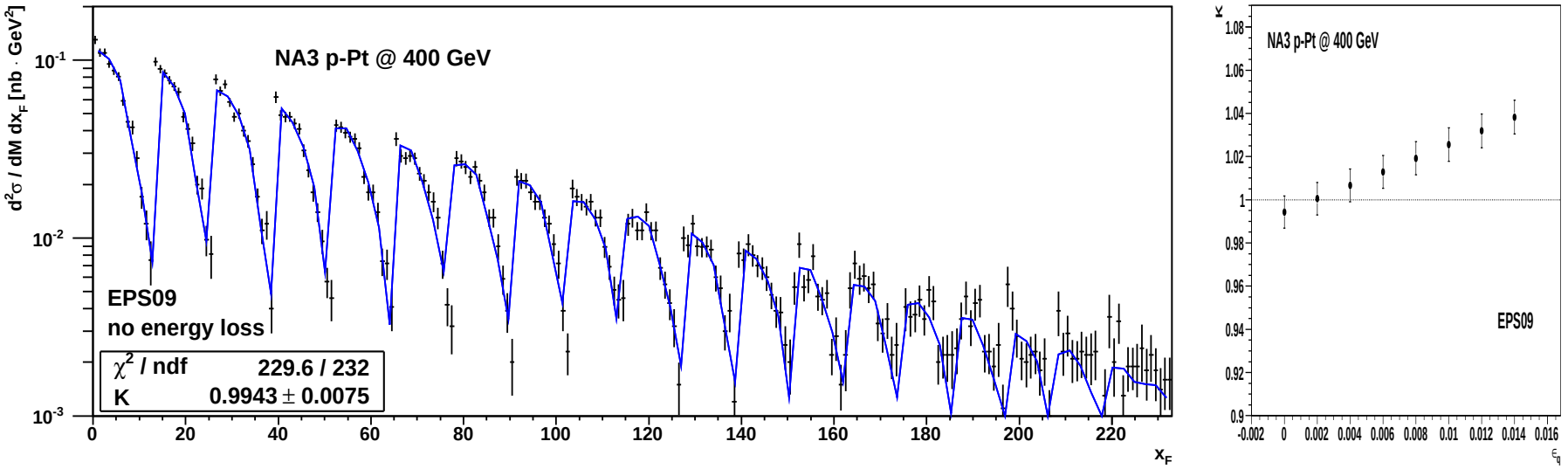

Figure 21: Left: The invariant DY cross section in pPt collisions at 400 GeV as a function of x_F in different mass bins with EPS09 nPDFs. Right: The K factors found in comparison to the data with various values of the energy loss parameter ϵ_q.

Shadowing vs. Isospin Effects on Drell-Yan I: Isospin

Large pPt/pp ratio without shadowing for $4 < M < 9$ GeV, ratio increases with M as x_1 increases and difference between u and d valence quarks is large

At higher energies, isospin effects are smaller in the same mass range because the x values will be lower, moving into the region where sea quark distributions dominate the u and d distributions

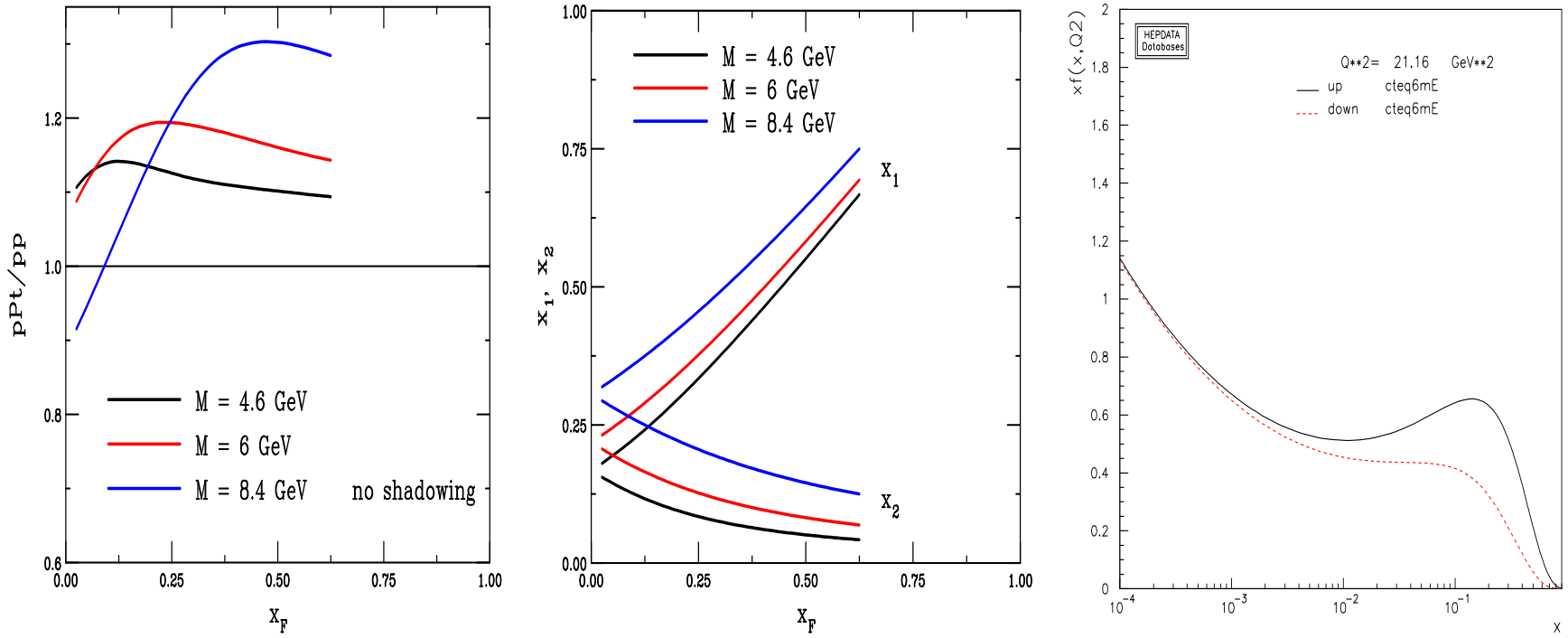

Figure 22: Left: The 400 GeV pPt/pp ratio for Drell-Yan production in several different mass bins as a function of x_F with no shadowing. Center: The x_1 and x_2 values for the same masses. Right: The CTEQ6M up (solid black) and down (dashed red) distributions at $M = 4.6$ GeV.

Shadowing vs. Isospin Effects on Drell-Yan II: Shadowing

At 400 GeV and $4 < M < 9$ GeV, the pPt/pp ratio with shadowing is nearly independent of x_F, x_2 covers range of antishadowing peak for valence quarks, mostly in shadowing region for sea quarks

Shadowing is nearly independent of whether light quark is up or down flavored

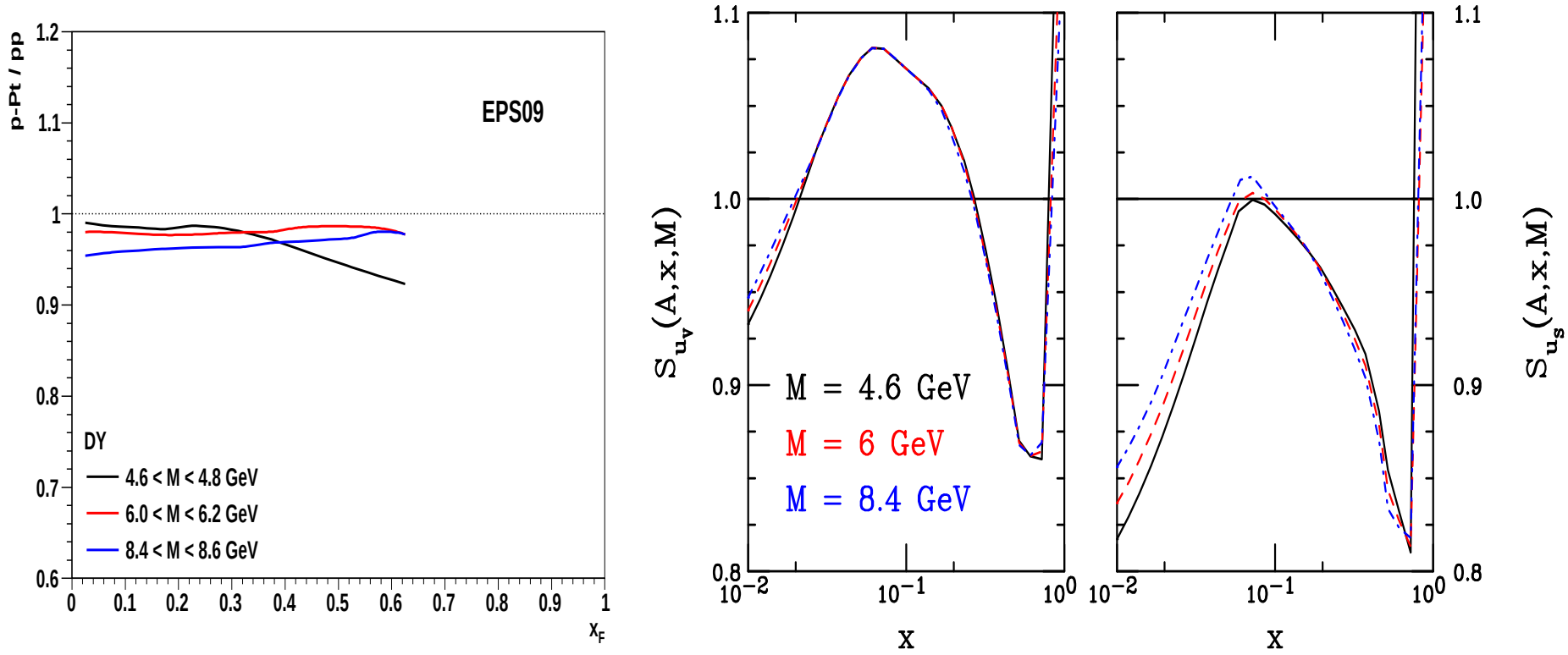

Figure 23: Left: The 400 GeV pPt/pp ratio for Drell-Yan production in several different mass bins as a function of x_F with the central EPS09 nPDF. Right: EPS09 central shadowing ratios for valence (left) and sea (right) quarks.

Adding Initial State Energy Loss to J/ψ Production

Rather large EPS09 uncertainty reduced in ratios; clearly initial-state shadowing is insufficient to describe effect

Combination of shadowing and energy loss with relatively x_F-independent absorption compares relatively well with the data for $x_F > 0.2$; HOWEVER, the assumed ϵ_q is much larger than found for Drell-Yan production

Stronger absorption closer to target? Formation time effects not yet included

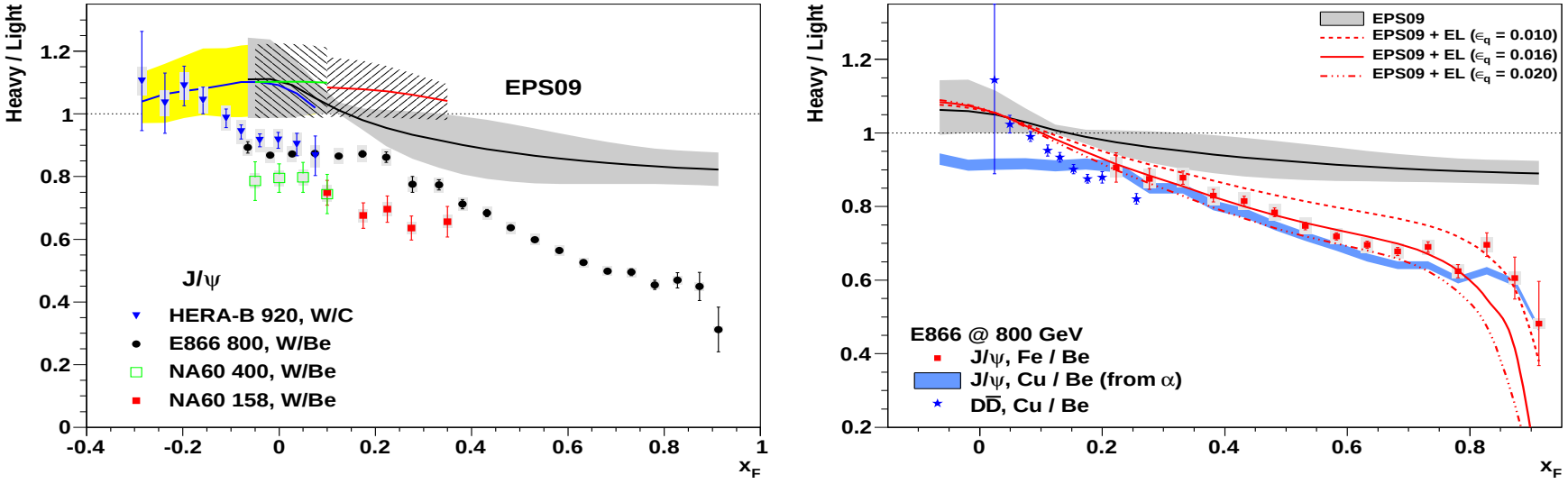

Figure 24: Left: The heavy to light ratios for W/Be in fixed target interactions. Right: Convolution of shadowing, absorption and various strengths of initial-state energy loss by quarks compared to the E866 data.

Summary .

- **CEM agrees well with RHIC and preliminary LHC data; useful tool for studying cold nuclear matter effects**
- **Data seem to suggest absorption cross section decreases with $\sqrt{s_{NN}}$ and increases at forward x_F, obviously effects still unaccounted for**
- **Study well-understood Drell-Yan production to get a handle on energy loss mechanism .**
- **J/ψ pA data seem to indicate stronger energy loss effects than needed for Drell-Yan production**